Early Circulating Tumor DNA Kinetics as a Dynamic Biomarker of Cancer Treatment Response

Aaron Li, MS[1]; Emil Lou, MD, PhD[2,3]; Kevin Leder, PhD[4]; and Jasmine Foo, PhD[1,2]

DOI https://doi.org/10.1200/CCI-24-00160

ABSTRACT

PURPOSE Circulating tumor DNA (ctDNA) assays are promising tools for the prediction of cancer treatment response. Here, we build a framework for the design of ctDNA biomarkers of therapy response that incorporate variations in ctDNA dynamics driven by specific treatment mechanisms. These biomarkers are based on novel proposals for ctDNA sampling protocols, consisting of frequent sampling within a compact time window surrounding therapy initiation—which we hypothesize to hold valuable prognostic information on longer-term treatment response.

METHODS We develop mathematical models of ctDNA kinetics driven by tumor response to several therapy classes and use them to simulate randomized virtual patient cohorts to test candidate biomarkers.

RESULTS Using this approach, we propose specific biomarkers, on the basis of ctDNA longitudinal features, for targeted therapy and radiation therapy. We evaluate and demonstrate the efficacy of these biomarkers in predicting treatment response within a randomized virtual patient cohort data set.

CONCLUSION This study highlights a need for tailoring ctDNA sampling protocols and interpretation methodology to specific biologic mechanisms of therapy response, and it provides a novel modeling and simulation framework for doing so. In addition, it highlights the potential of ctDNA assays for making early, rapid predictions of treatment response within the first days or weeks of treatment and generates hypotheses for further clinical testing.

ACCOMPANYING CONTENT

Data Supplement

Accepted January 7, 2025
Published March 7, 2025

JCO Clin Cancer Inform
9:e2400160
© 2025 by American Society of Clinical Oncology

Creative Commons Attribution Non-Commercial No Derivatives 4.0 License

INTRODUCTION

Circulating tumor DNA (ctDNA) assays—which detect cell-free DNA fragments released by tumor cells into the bloodstream—are a sensitive, noninvasive approach to assessing tumor burden and genomic profiles without biopsy. Serial ctDNA kinetics have also been explored as a possible predictor of response to treatment in a variety of cancer types, such as colorectal cancer[1-5] and non–small cell lung cancer.[6-9] Some features of ctDNA longitudinal dynamics, such as the existence of transient peaks in ctDNA levels, rapid clearance rates during therapy, or lower ctDNA levels at baseline or a month after therapy, have been correlated with treatment efficacy.[3,10-15] Specific features of these early data vary greatly between different treatment types,[10] suggesting that any longitudinal biomarkers designed for interpreting early ctDNA dynamics should be specific to therapeutic class and mechanism of action.

Currently, serial ctDNA data studies typically collect samples several months apart. Since the production and clearance kinetics of ctDNA in the bloodstream occur on relatively faster time scales (hours, minutes),[16,17] this spacing may overlook crucial early indicators of treatment response. Sanz-Garcia et al[10] provide an excellent review of the existing data on ctDNA kinetics and biomarker trials under various types of treatment, and Table 1 shows a partial summary of existing studies on ctDNA biomarkers. These studies not only demonstrate significant potential in the use of ctDNA analyses for prognostic predictions but also highlight the need for increased prediction accuracy and an improved understanding of how early ctDNA dynamics vary across treatment types.

In this study, we explore the potential of early ctDNA dynamics as a prognostic indicator of treatment efficacy, using mathematical modeling as a conceptual tool. We develop mathematical models for ctDNA dynamics under targeted therapy, chemotherapy, and radiotherapy, and leverage these models to explore how ctDNA kinetics vary between therapy classes. These results build upon the growing literature on mathematical and computational models of ctDNA dynamics.[2,8,23,24] For example, Avanzini et al[25] introduced a mathematical model of ctDNA dynamics in

CONTEXT

Key Objective

How can circulating tumor DNA (ctDNA) be used for the early prediction of treatment response, and how should treatment mechanism influence the interpretation of ctDNA dynamics?

Knowledge Generated

The current study establishes a general framework for the design of treatment-specific biomarkers for guiding the sampling and interpretation of ctDNA analyses, on the basis of mechanistic modeling and the generation of virtual randomized patient cohorts. Longitudinal ctDNA biomarkers for predicting treatment response were identified for targeted therapy, chemotherapy, and radiation using mathematical models.

Relevance

Frequent, early ctDNA sampling on the basis of a mechanistic understanding of therapy-driven tumor dynamics may enable rapid identification of patients who are likely to benefit from a specific treatment. Such tailored ctDNA biomarker strategies could guide timely treatment modifications, potentially improving patient outcomes and reducing unnecessary treatment exposure.

untreated tumors and estimated the increase in detection lead time afforded by ctDNA analyses over imaging. Here, using simulated virtual patient cohorts, we develop dynamic biomarkers predictive of treatment response using early, frequent ctDNA sampling. We demonstrate that these biomarkers, on the basis of mechanistic biologic principles, perform equally as well as standard neural network approaches while retaining mechanistic interpretation. These modeling results suggest that *frequent ctDNA collection in the initial stages of treatment* may provide early indicators of whether treatment will be successful.

METHODS

Impact Of Therapeutic Mechanisms On ctDNA Dynamics

We first explore how therapeutic mechanisms of action may drive differences in ctDNA dynamics. We develop mathematical models of ctDNA kinetics arising from tumor cell population responses to targeted therapy, chemotherapy, and radiotherapy and examine how these mechanisms drive distinct features in ctDNA data. For simplification, we will refer to and define all cytotoxic traditional forms of systemic chemotherapies using the term "chemotherapy" and use "targeted therapy" to refer to molecularly targeted agents including small-molecule inhibitors.

Targeted Therapy

We consider a mechanistically motivated model of ctDNA shedding under cytotoxic targeted therapy, as described in Figure 1A. Therapies often fail because of the emergence of drug-resistant cell subpopulations; thus, we incorporate both drug-sensitive and drug-resistant subpopulations within the model. Each population evolves as a stochastic birth-death process, where cells divide and die stochastically with exponentially distributed waiting times governed by their respective birth and death rates, which may vary according to cell type and drug concentration. Specifically, the drug-sensitive population has birth rate $b_{s,1}$, death rate $d_{s,1}$, and net growth rate $\lambda_{s,1} \equiv b_{s,1} - d_{s,1}$ in the absence of drug; it has birth rate $b_{s,2}$, death rate $d_{s,2}$, and net growth rate $\lambda_{s,2} \equiv b_{s,2} - d_{s,2}$ in the presence of drug. We assume that this population on average expands in the absence of therapy and declines in the presence of drug (ie, $\lambda_{\{s,1\}} > 0 > \lambda_{\{s,2\}}$). The drug-resistant population has birth rate $b_{r,1}$, death rate $d_{r,1}$, and net growth rate $\lambda_{r,1} \equiv b_{r,1} - d_{r,1}$ in the absence of drug; it has birth rate $b_{r,2}$, death rate $d_{r,2}$, and net growth rate $\lambda_{r,2} \equiv b_{r,2} - d_{r,2}$ in the presence of drug. We assume that therapy can affect the growth of drug-resistant cells, but that the drug-resistant population increases on average, in both the presence and the absence of drug (ie, $\lambda_{\{r,1\}} \geq \lambda_{\{r,2\}} > 0$).

Similar to the study by Avanzini et al,[25] to model the process of ctDNA production, we assume that during each cell death from either population, one human genome equivalent (hGE) of ctDNA is shed into the bloodstream with probability q. The ctDNA is eliminated from the bloodstream at random exponential rate ε. We assume that the modeled ctDNA tracks a generic tumor genomic marker that does not distinguish whether the ctDNA originated from the drug-sensitive or drug-resistant subpopulation; future work will consider more detailed models of individual mutational frequencies. In our treatment model, cytotoxic drug is applied continuously starting at time 0 and may alter the birth and death rates of the tumor subpopulations. Under this model, we derive summary statistics for the abundance of ctDNA under treatment, which are available in the Data Supplement.

 © 2025 by American Society of Clinical Oncology

TABLE 1. A Partial Summary of ctDNA Biomarker Analysis in Targeted Therapy, Chemotherapy, and Radiotherapy

Author(s)	Treatment Type	No.	Time Points	Biomarker Definition	Efficacy
Parikh et al[11]	Targeted therapy	138	Baseline, 2, 4, 8, and 16 weeks	Decrease from baseline to week 4	Predicted clinical benefit at a 90% specificity and a 60% sensitivity
Vidal et al[18]	Chemotherapy and targeted therapy	100	Baseline and C3 (week 4-6)	Decrease from baseline	Correlation with PFS (HR, 0.23, P = .001)
Magbanua et al[19]	Chemotherapy	295	Baseline, 3 and 12 weeks, post-treatment	Concentration, clearance, and others	Early clearance correlated with pathologic complete response (OR, 13.06, P = .0002)
Garlan et al[4]	Chemotherapy	82	Baseline, 2 and 4 weeks	Concentration at baseline, decrease from baseline	Dividing patients into good and bad ctDNA responders. Good responders had better objective response rate (41.3%) than bad responders (0%)
Tie et al[3]	Chemotherapy	53	Baseline, day 3, and days 14-21	≥10-fold reduction from baseline	Seventy-four percent with -≥10 fold had radiologic response, compared with only 35% of patients with lesser reductions
Leung et al[20]	Radiotherapy and chemoradiotherapy	107	Baseline, 4 weeks, and post-treatment	Detectable ctDNA at 4 weeks	Correlated with worse PFS (HR, 4.05, P = .0001)
Chera et al[21]	Chemo-radiotherapy	103	Baseline, 1, 2, 3, and 4 weeks	Favorable clearance profile: high baseline and >95% clearance by day 28	Nineteen of 67 patients had favorable clearance profiles: none had persistent or recurrent disease. Thirty-five percent of patients with unfavorable profiles had persistent or recurrent disease (P = .0049)
Lv et al[22]	Radical induction chemotherapy and chemoradiotherapy	673	One sample per cycle for four cycles	Used supervised statistical clustering to create four prognostic phenotypes	Clusters associated with different risks of tumor relapse

Abbreviations: ctDNA, circulating tumor DNA; HR, hazard ratio; OR, odds ratio; PFS, progression-free survival.

Figure 2A shows an example simulation of a tumor population that not only initially consists primarily of drug-sensitive cells but also harbors a small resistant subpopulation. On application of treatment at time 0, the tumor population decreases and is accompanied by a sharp increase in ctDNA followed by a gradual decrease in ctDNA below baseline levels; this transient peak arises because of the sharp increase in cell apoptosis at the start of therapy application, resulting in a significant amount of released ctDNA. If the initial resistant subpopulation frequency is increased, the size of the initial peak is decreased (Fig 2C). Similarly, increasing drug effectiveness on the sensitive cell population results in higher initial peaks (Figs 2D), suggesting that the presence and magnitude of transient peaks may be predictive of responsiveness in targeted therapy. Although data sets with sufficiently frequent, early samples of ctDNA are too rare to fully parametrize and validate this model, we fitted our model to evaluate consistency with one existing longitudinal data set. Riediger et al[12] examined daily ctDNA levels in a patient with non–small cell lung cancer treated with tyrosine kinase inhibitors. The patient responded well to treatment and exhibited an 11-fold peak in ctDNA levels at 26 hours followed by a subsequent decrease. An example fitting of our derived expectation for ctDNA under the targeted model with these data is shown in Figure 2B. Similarly, Husain et al[13] observed spikes in ctDNA levels in the first week of therapy in eight patients with non–small cell lung cancer who exhibited clinical benefit from osimertinib.

The targeted therapy model can also be adapted to model ctDNA kinetics under chemotherapy. Under the chemotherapy model, a birth event of a sensitive cell has probability K_s of becoming a death event instead and the birth event of a resistant cell has probability K_r of converting to a death. This results in birth and death rates

$$b_{s,2} = b_{s,1}(1 - K_s),$$

$$d_{s,2} = d_{s,1} + b_{s,1}K_r,$$

$$b_{r,2} = b_{r,1}(1 - K_r),$$

$$d_{r,2} = d_{r,1} + b_{r,1}K_r,$$

for the sensitive and resistant cells. Thus, the chemotherapy model is a special case of the targeted therapy model where the changes in the birth and death rates are dictated by K_s and K_r.

The behavior of the chemotherapy model is similar to that of the targeted therapy model, with responsive patients exhibiting ctDNA peaks followed by gradual declines. However, for parameters yielding similar tumor dynamics, chemotherapy yields a smaller peak in ctDNA (Figs 2E and 2F). Clinically, Tie et al[3] observed moderate ctDNA spikes at day 3 (≤three-fold), followed by a rapid decline in three patients with metastatic colorectal cancer who exhibited tumor reduction from chemotherapy.

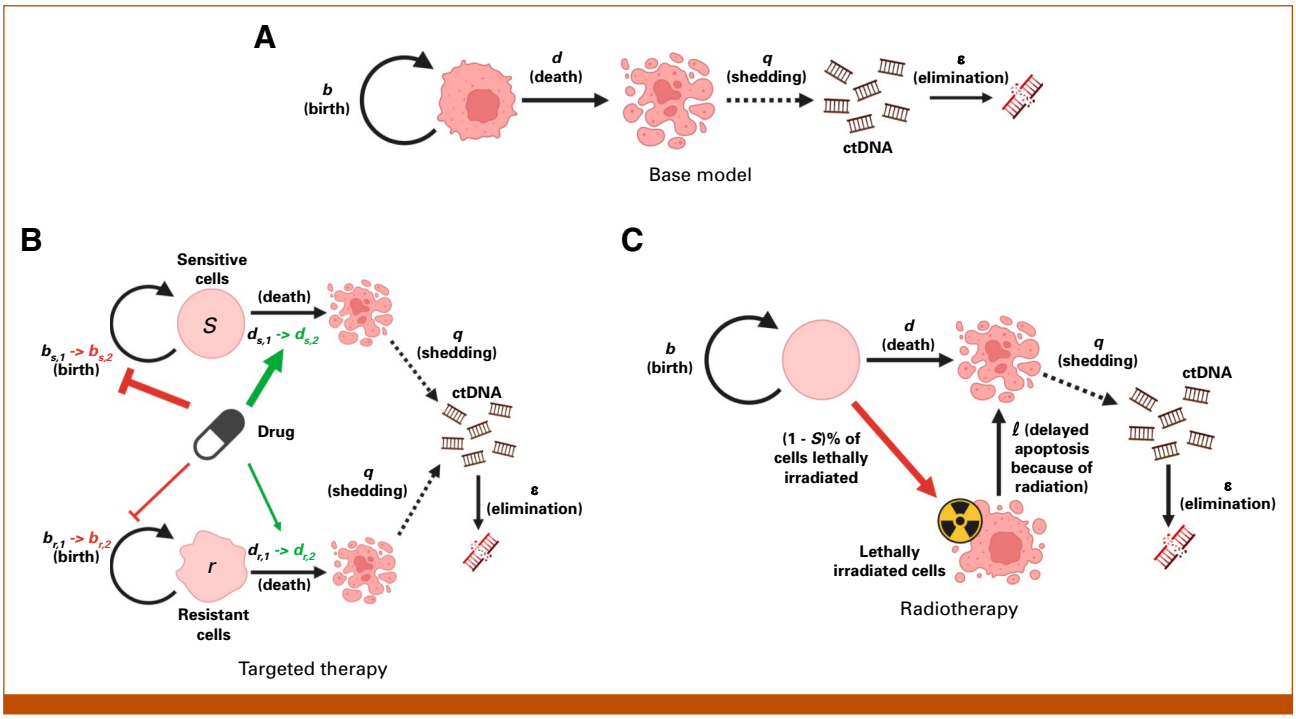

FIG 1. Schematics of models for ctDNA kinetics: baseline without treatment, targeted therapy, and radiotherapy. Created in BioRender.com. (A) Base model: Without treatment, the tumor population is modeled as a stochastic birth-death process, starting with an initial population with birth rate b and death rate d. For each cell death, one hGE of ctDNA is released with probability q. ctDNA is eliminated from the bloodstream at rate ε. (B) Targeted therapy model: Initial tumor population consists of a mixture of sensitive and resistant cells, modeled as stochastic birth-death processes with (untreated) birth and death rates $b_{s,1}, d_{s,1}$ and $b_{r,1}, d_{r,1}$, respectively, off drug. Under therapy, the birth and death rates of the populations change to $b_{s,2}, d_{s,2,}$ and $b_{r,2}, d_{r,2}$, respectively. (C) Radiotherapy model: Initial population of cells with birth rate b and death rate d. For each dose of radiotherapy, S is the proportion of cells that survive each treatment. The remaining $(1 - S)$ proportion of cells are lethally irradiated cells which can no longer divide and instead die at rate l, at which point they release ctDNA with probability q. ctDNA, circulating tumor DNA; hGE, human genome equivalent.

Radiotherapy

We developed a model of ctDNA dynamics driven by tumor responses to radiation therapy delivered in fractionated doses. The tumor population $N(t)$ is modeled by a stochastic birth-death process as in our base model, with each death accompanied by probability q of shedding 1 hGE of ctDNA. Fractionated radiation treatments are applied at times $\{t_1, ..., t_n\}$. The effect of each dose is modeled with the well-established[26] linear quadratic cell kill model, where the survival probability of a cell after treatment with dosage D Gray is given by $S = e^{\{-\alpha D - \beta D^2\}}$.[27] For each dose, $SN(t_i)$ of the cells survive and are unaffected and $(1 - S)N(t_i)$ become lethally irradiated cells, which die off at rate l and can no longer divide. Derivations of summary statistics for the abundance of ctDNA under radiotherapy treatment are available in the Data Supplement.

Figure 3A shows an example simulation of the radiotherapy model with a fractionation schedule (vertical gray lines) of four cycles of weekday treatments starting on day 7. Under this model, the ctDNA dynamics gradually peak several days after the first treatment date and exhibit a slow decline afterward that tracks the tumor burden decline. We have not considered a radioresistant subpopulation in this model yet; thus, partial response (PR) indicates eventual complete response. Figure 3C shows ctDNA kinetics for simulations with varying values of S, the survival fraction. Increased treatment efficacy results in a larger increase over the first week of treatment and a greater decrease in the second week of treatment. Figure 3D shows simulations for varying l^{-1} values, which represents the mean lag time between irradiation and cell death/ctDNA release. Lower lag times result in increased ctDNA during the first week of treatment.

The kinetics of ctDNA under radiation treatment are summarized in a review by McLaren and Aitman[28] and support predictions from our mechanistic model. As in targeted therapy and chemotherapy, radiotherapy patients have exhibited transient rises in ctDNA followed by eventual decreases within 2 weeks of treatment initiation.[15,29,30] However, in contrast to the ctDNA peaks observed at 26 hours in targeted therapy,[12] peak ctDNA levels from radiation treatment have generally been observed 3-6 days after the first treatment in both xenograft models[29] and patients with human nasopharyngeal carcinoma.[15]

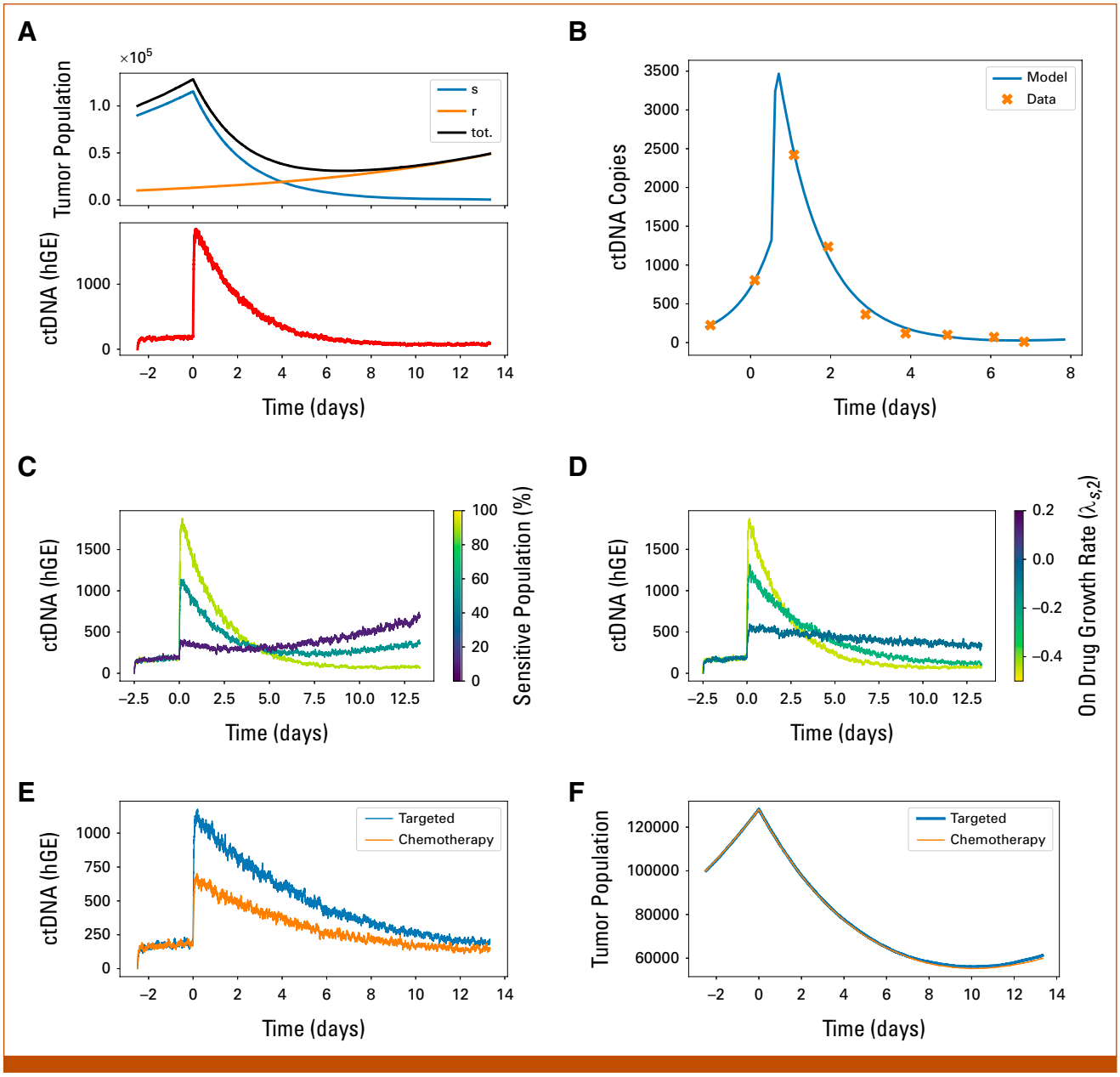

FIG 2. Exploration of the targeted therapy model. (A) Example simulation for the targeted therapy model. The simulation begins with 10^5 total cells, 90% of which are drug-sensitive. The ctDNA shedding rate is set to $q = 1$, and the elimination rate is set to $\varepsilon = 33$ per day. Off drug, the birth rate is $b_{-,1} = 0.15$ per day and death rate is $d_{-,1} = 0.05$ per day for both drug-sensitive and drug-resistant cells. Treatment is started when the tumor increases in population by 25%. On treatment, the birth and death rates for the drug-sensitive cells become $b_{s,2} = 0.1$, $d_{s,2} = 0.55$, whereas the rates for the drug-resistant cells are unchanged. (B) Example linear regression fitting of our targeted therapy model to ctDNA data from a patient with NSCLC treated with afatinib obtained by Riediger et al.[12] The blue line denotes the expected ctDNA levels $E[C(t)]$ (see the Data Supplement) produced by the best fit parameters, and the orange crosses denote ctDNA samples from patient data. (C and D) Example ctDNA simulations for varying initial proportions of sensitive cells and drug efficacy. (C) shows simulations for proportions of 90%, 50%, and 10% sensitive cells. (D) shows simulations for varying death rate on drug resulting in values for $\lambda_{s,2}$ of -0.45, -0.25, and 0.05 per day. The initial parameters of the simulations are the same as in (A) otherwise. (E and F) A comparison of ctDNA levels from simulations of the targeted therapy model with $d_{s,2} = 0.32$ and the chemotherapy model with $K_s = 0.9$. Both simulations have the same net growth rates on and off drug $\lambda_{s,1} = 0.1$ and $\lambda_{s,2} = -0.17$. ctDNA, circulating tumor DNA; hGE, human genome equivalent; NSCLC, non–small cell lung cancer.

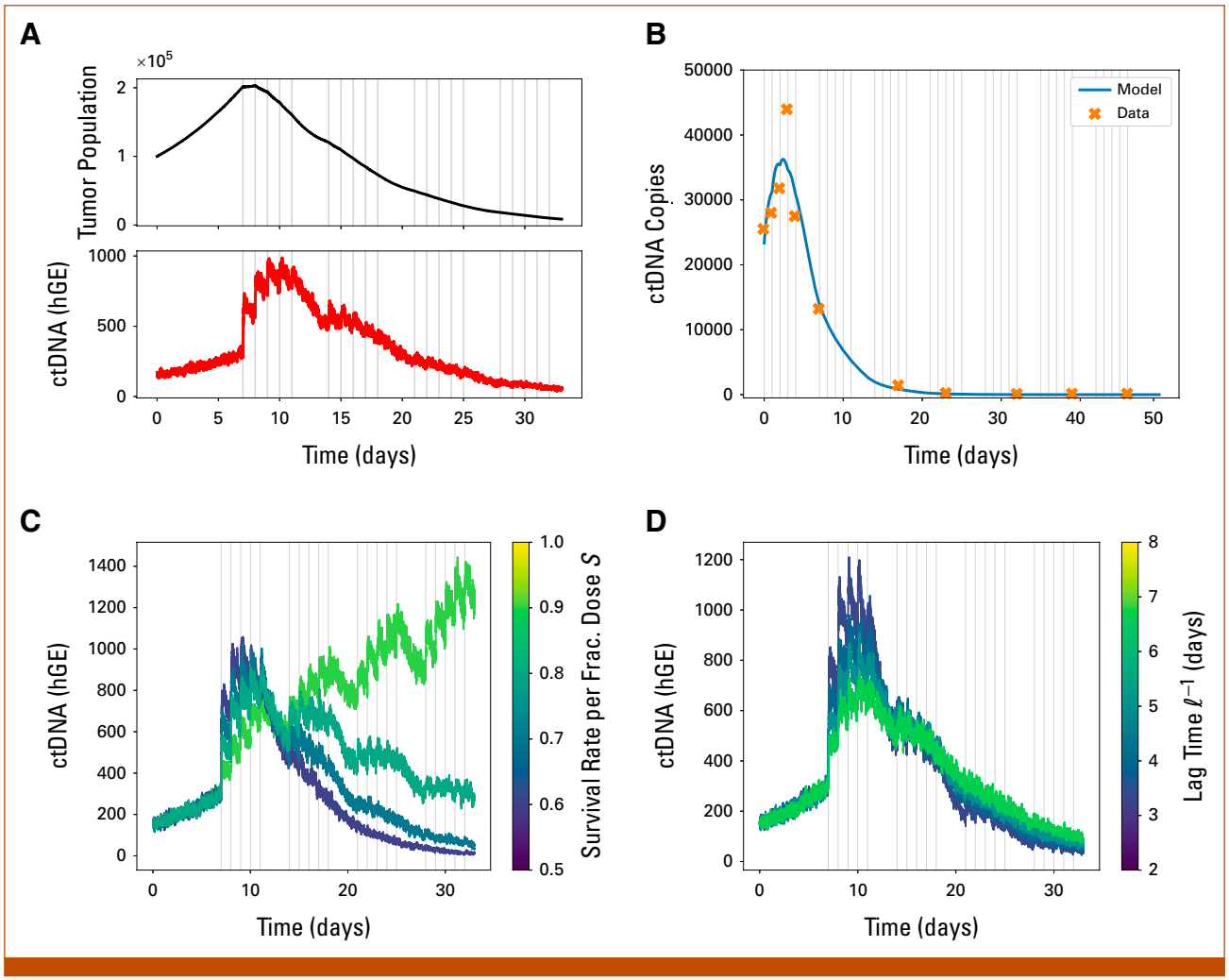

FIG 3. Exploration of the radiotherapy model. (A) Example simulation starting with 10^5 initial cells, birth and death rates $b = 0.15$, $d = 0.05$, elimination rate $\varepsilon = 33$, and shedding rate $q = 1$. Fractionated radiotherapy doses are applied in a 5-day on, 2-day off schedule starting on day 7. Each dose has survival rate $S = 0.7$. The lag parameter is $l = 0.25$, corresponding to a mean lag time of 4 days before ctDNA release from doomed irradiated cells. (B) Example linear regression fitting to patient data from the study by Lo et al[15] to the mean model–predicted ctDNA level (Data Supplement). (C and D) Example simulations for varying survival rates and lag times. In (C), the survival rate per fractionated dose S is varied from 0.6 to 0.9. In (D), the lag time is varied from 3 to 7 days. The initial parameters are the same as in (A) otherwise. ctDNA, circulating tumor DNA; hGE, human genome equivalent.

RESULTS

Biomarker Design Using Virtual Patient Cohorts

We next use our models of treatment response to propose and evaluate various candidate biomarkers of response to each therapy, with the goal of early treatment response prediction. Table 1 shows the existing ctDNA biomarker analyses, indicating not only the potential of ctDNA assays for prognostic prediction but also inconsistency in biomarker design and efficacy across cancer and treatment types. Current ctDNA biomarker usage is limited by the lack of higher time resolution data and the focus on the decrease in ctDNA alone as a prognostic indicator. A few case studies with daily ctDNA sampling during the beginning of treatment exhibit interesting features such as transient ctDNA peaks in responsive patients.[3,12,15] Rational biomarker design, on the basis of a quantitative, mechanistic models of treatment effects and ctDNA dynamics, has the potential to leverage these features for making personalized and rapid treatment decisions. However, no such data are currently available for larger groups of patients. Thus, here, we use the models developed in the Impact of Therapeutic Mechanisms on ctDNA Dynamics section to simulate randomized virtual patient cohorts with higher time resolution early ctDNA sampling for the development of treatment mechanism-specific biomarkers that predict treatment response.

 © 2025 by American Society of Clinical Oncology

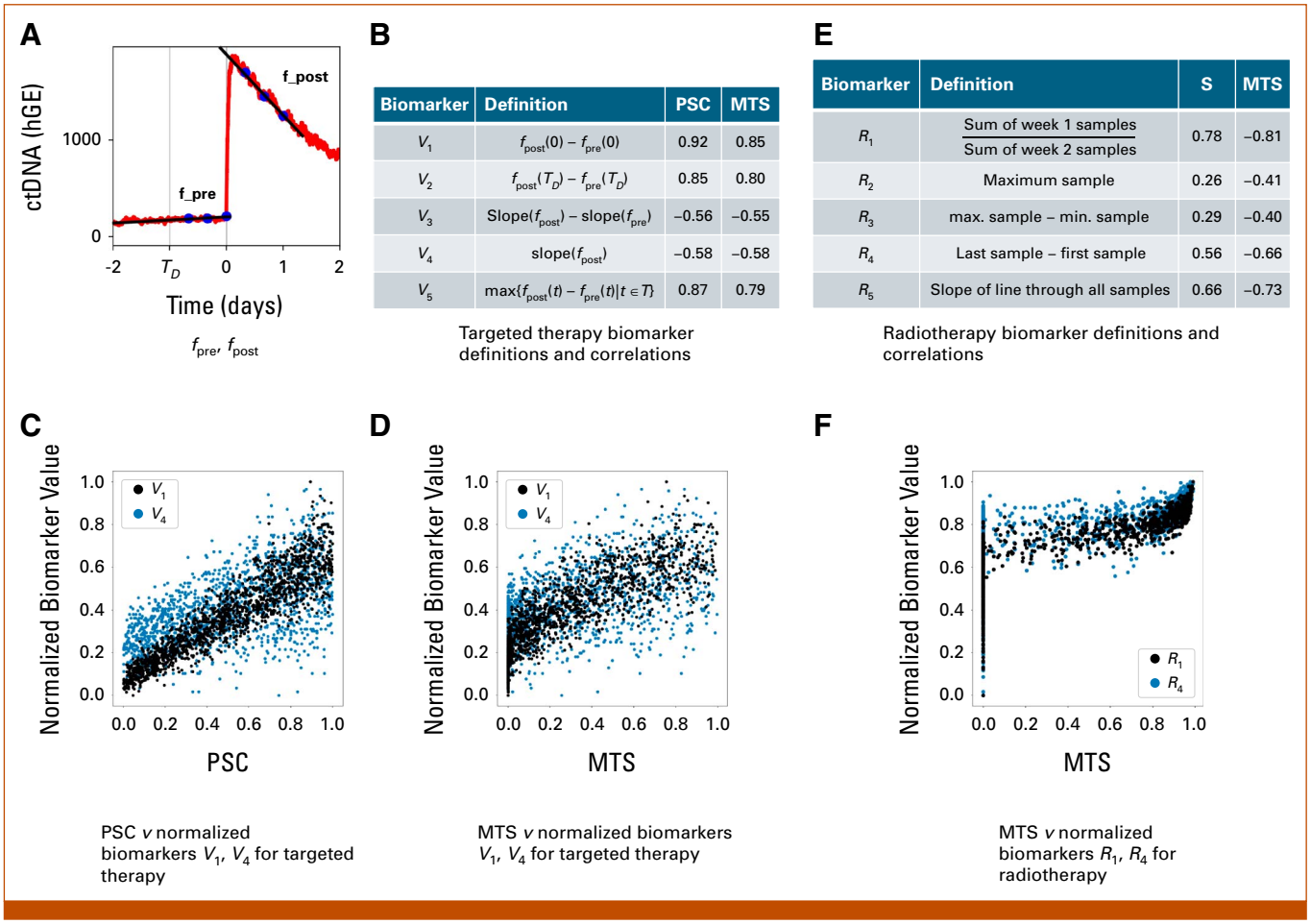

FIG 4. (A-D) Biomarker definitions and analysis for targeted therapy. (A) Example diagram for f_{pre}, f_{post}. We fit lines f_{pre}, f_{post} to the samples before and after initiation of treatment, respectively (blue dots). (B) Table of biomarker definitions and correlation coefficients of biomarkers and the initial PSC and the MTS, that is, the largest proportional decrease in tumor burden, for a cohort of 1,500 simulated patients with random parameters. The time of detection is denoted T_d and is equal to -1 in this simulation. The set of sample times after the start of treatment are denoted T. (C and D) Correlations of PSC and MTS with normalized biomarker values for V_1, V_4, in the simulated cohort. Each biomarker was scaled to have values within $[0, 1]$. (E and F) Biomarker definitions and analysis for radiotherapy. (E) Table of biomarker definitions and correlation coefficients of biomarkers with S, the survival probability for each fractionated dose and the MTS, that is, the largest proportional decrease in tumor burden, for a cohort of 1,000 simulated patients with random parameters. ctDNA samples were collected on Monday, Wednesday, and Friday of the first 2 weeks of treatment (days 7, 9, 11, 14, 16, 18). (F) Correlations of MTS with normalized biomarker values for the R_1, R_4 insimulated cohort. Each biomarker was scaled to have values within $[0, 1]$. ctDNA, circulating tumor DNA; MTS, maximum tumor shrinkage; PSC, proportion of sensitive cells.

Targeted Therapy Biomarkers

The targeted therapy model from the Targeted Therapy section was used to generate a randomized cohort of 1,500 patients treated with targeted cytotoxic treatment. Details of the randomized cohort generation are provided in the Data Supplement. We simulated a dense data collection protocol, taking three evenly spaced ctDNA samples in the 24 hours immediately before and three samples immediately after the start of treatment, and explored the development of biomarkers using these sampled data to predict treatment response.

We consider two primary components as building blocks for biomarker design: f_{pre} and f_{post}, lines fit to the samples before and after treatment initiation, respectively (Fig 4A). These components were then combined in several different candidate biomarkers (Fig 4B) and assessed for predictive ability. These candidates were assessed on the basis of their correlation strength with clinically relevant metrics, the initial proportion of sensitive cells (PSC), and the maximum tumor shrinkage (MTS). The Data Supplement (Figs S1 and S2) shows the correlations between each biomarker candidate and MTS or PSC, and the table in Figure 4B summarizes the correlation coefficients. The most effective biomarker in this analysis was V_1, a metric for the height of the jump in ctDNA levels on initiation of treatment. These results suggest that larger height of the ctDNA peak induced by the start of targeted

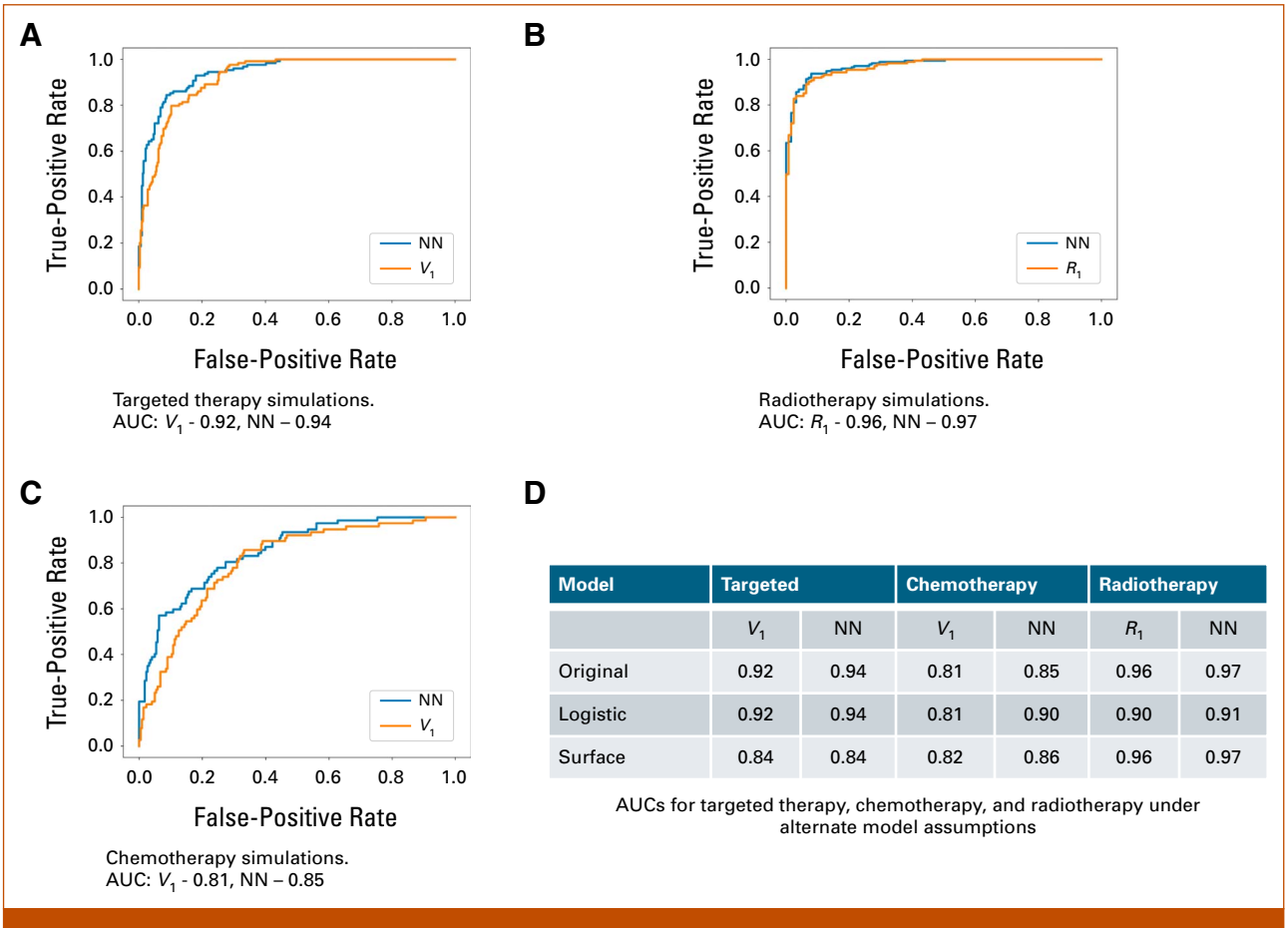

Model	Targeted		Chemotherapy		Radiotherapy	
	V_1	NN	V_1	NN	R_1	NN
Original	0.92	0.94	0.81	0.85	0.96	0.97
Logistic	0.92	0.94	0.81	0.90	0.90	0.91
Surface	0.84	0.84	0.82	0.86	0.96	0.97

AUCs for targeted therapy, chemotherapy, and radiotherapy under alternate model assumptions

FIG 5. Detection of partial response (tumor shrinkage of at least 20%) in simulated random cohorts. (A-C) ROC curves for prediction of PR from simulated ctDNA data for candidate biomarkers (V_1, R_1) and for NN classifiers. ROC curves are shown for (A) 1,500 simulated targeted therapy patients, (B) 1,000 simulated radiotherapy patients, and (C) 1,000 simulated chemotherapy patients. (D) In addition to the simulations under the original model assumptions, simulated cohorts for each treatment type were generated with models accounting for logistic growth with a carrying capacity and the assumption of spherical tumors with only surface cells shedding ctDNA. ctDNA, circulating tumor DNA; NN, neural network; PR, partial response; ROC, receiver operating characteristic.

cytotoxic therapy should be correlated with a stronger tumor reduction.

Radiation Therapy Markers

The radiation therapy model from the Radiotherapy section was used to generate a randomized cohort of 1,000 patients treated with radiation. Details of the randomized cohort generation are provided in the Data Supplement. The patients were treated with a 4-week schedule of daily weekday radiation doses starting on day 7. ctDNA samples were collected on Monday, Wednesday, and Friday of the first 2 weeks of treatment (days 7, 9, 11, 14, 16, and 18). This extended sampling window, in comparison with targeted therapy, is motivated by effects of the lag time between radiation and apoptosis of lethally irradiated cells, observed clinically[15] and in simulations (Fig 3D).

Using these simulated cohort data, several candidate biomarkers were explored using features of the sampled ctDNA dynamics. Figure 4E provides definitions of candidate biomarkers, which were evaluated by examining their correlation with the survival probability S of each cell after each fractionated dose of radiation (which measures efficacy of treatment), and the MTS in the simulated cohort. By this measure, the most predictive biomarker was R_1, which approximates the AUC in the second treatment week divided by the AUC of the first week.

Biomarker Performance in Predictions of PR

To further evaluate the performance of the top candidate biomarkers (V_1, R_1), we assessed their ability to predict whether simulated patients would achieve at least PR, that is, at least a 30% decrease in tumor burden during treatment (MTS ≥ 0.3). Note that simulated patients who achieve complete response are considered in the PR group for this study. Figure 5 shows the receiver operating characteristic (ROC) curves for detection of PR in the simulated cohorts of patients undergoing targeted cytotoxic therapy, chemotherapy, and radiation. In each case,

the top candidate biomarkers showed strong ability to predict PR. Using V_1 with our simulated targeted therapy cohort data resulted in an ROC curve (Fig 5A) with an AUC of 0.92 for detection of PR. In particular, the optimal threshold of $V_1 \geq 76$ predicted PR with an 87% sensitivity, an 88% specificity, and an 81% positive predictive value. The V_1 biomarker was also evaluated as a predictor of PR for a randomly simulated cohort of 1,000 randomly assigned chemotherapy patients. We found that this produced an ROC curve with AUC 0.81 (Fig 5B). At the optimal threshold of $V_1 \geq 29$, PR was predicted with an 80% sensitivity, a 74% specificity, and a 61% positive predictive value (PPV). Finally, R_1 was evaluated as a classifier of PR in a simulated radiotherapy cohort of 1,000 patients; this produced an ROC curve with AUC 0.96 (Fig 5C). The optimal threshold was found to be $R_1 \leq 1.15$, which predicted PR with a 91% sensitivity, a 91% specificity, and a 93% PPV. Overall, the top-performing biomarkers (V_1, R_1) for targeted therapy, chemotherapy, and radiotherapy demonstrated strong performance in predicting PR.

Comparison With Neural Network Classifiers and Model Generalizations

To investigate additional ctDNA features not captured by these biomarkers that may improve prediction, we trained and tested a three-layer neural network classifier implemented in PyTorch on the same randomized cohort data used for the biomarker analyses. The classifier was designed to receive a patient's ctDNA samples as input and predict whether the patient would exhibit PR. The performance of our proposed biomarkers was able to match that of the neural network classifier (Fig 5), with the AUC matching that of the classifier closely for all three treatment types. This suggests that the proposed biomarkers are optimal or near optimal, while retaining interpretability.

The performance of the proposed biomarkers against the neural network classifier was also assessed under alternate model assumptions (Data Supplement) and with reduced samples (Data Supplement, Fig S5). In our base model, the tumor is assumed to be small relative to carrying capacity, so that growth is not limited and ctDNA shedding can originate from any cell. To analyze the validity and robustness of our observations, we tested our proposed biomarkers using simulations under logistic growth with a carrying capacity and surface-only ctDNA shedding. In both cases, V_1 was still the best predictor for targeted therapy and chemotherapy and R_1 was still the best biomarker for radiotherapy. In all scenarios, these biomarkers performed similar to the neural network classifier (Fig 5D). This suggests that the predictive power of these markers is robust to model assumptions. When omitting the first and last of the six ctDNA samples, the same biomarkers V_1, R_1 were still able to predict PR with high accuracy (AUC 0.89, 0.75, and 0.94 for targeted therapy, chemotherapy, and radiotherapy, respectively).

DISCUSSION

This study leverages mechanistic modeling of therapeutic response and simulated randomly assigned patient cohorts to develop ctDNA longitudinal biomarkers for predicting prognosis in tumors treated with targeted therapy, chemotherapy, and radiation therapy. In the case of cytotoxic targeted therapy and chemotherapy, V_1, a metric quantifying the height of initial ctDNA peaks successfully predicted future PR with AUCs of 0.92 and 0.81, respectively. For radiotherapy, the metric R_1, an approximation of the AUC in the second treatment week divided by the AUC of the first week, predicted PR with AUC 0.96. For all three treatment classes, dynamic early ctDNA biomarkers that performed favorably compared with existing biomarkers (Table 1) in terms of accuracy and earliness, in simulated patient cohorts, were identified. This biomarker performance was robust to alternate model assumptions such as surface-driven ctDNA shedding and resource-limited tumor growth. These results suggest that early ctDNA kinetics with sufficient time resolution have the potential to provide valuable predictions of clinical outcomes.

The proposed biomarkers rely on frequent ctDNA samples collected within a short time window surrounding the initiation of therapy. For targeted therapy or chemotherapy, the biomarker V_1 uses six samples collected during a 48-hour period (24 hours before and 24 hours after initiation of therapy). For radiotherapy, the quantity R_1 uses six samples collected during the first 2 weeks after initiation of radiotherapy. These proposed sampling approaches differ significantly from most current sampling protocols in clinical practice, where ctDNA is collected at time points occurring several weeks or months apart.[4,11,18,21] Our results suggest that early treatment ctDNA signals may hold valuable information about biologic response to therapy. The rapid time scales of ctDNA production and decay, which are driven by biologic and chemical processes occurring on the scales of hours and minutes, provide additional motivation for dense, frequent sampling within this early treatment period. Valuable prognostic information about tumor response to therapies could be overlooked under sampling protocols that are insufficiently dense or that miss the therapy induction window.

The current study establishes a general framework for the design of treatment-specific biomarkers for guiding the sampling and interpretation of ctDNA analyses, on the basis of mechanistic modeling and the generation of virtual randomly assigned patient cohorts. However, comparison with clinical observations, once available, is critical for evaluating and refining the specific biomarkers and sampling protocols proposed in this study. In addition, modeling of pharmacokinetics, combination therapies, and tumor-immune dynamics are the subject of the current work.

AFFILIATIONS

[1]School of Mathematics, University of Minnesota, Twin Cities, MN
[2]Masonic Cancer Center, University of Minnesota, Twin Cities, MN
[3]Division of Hematology, Oncology, and Transplantation, Department of Medicine, University of Minnesota, Twin Cities, MN
[4]Department of Industrial and Systems Engineering, University of Minnesota, Twin Cities, MN

PREPRINT VERSION

Preprint version available on bioRxiv (https://doi.org/10.1101/2024.07.01.601508).

CORRESPONDING AUTHOR

Jasmine Foo, PhD; e-mail: jyfoo@umn.edu.

SUPPORT

Supported by NSF DMS 2052465 (J.F., A.L.) and NSF CMMI 2228034 (J.F., K.L.).

AUTHOR CONTRIBUTIONS

Conception and design: All authors
Financial support: Jasmine Foo
Administrative support: Jasmine Foo
Provision of study materials or patients: Jasmine Foo
Collection and assembly of data: Aaron Li, Emil Lou
Data analysis and interpretation: All authors
Manuscript writing: All authors
Final approval of manuscript: All authors
Accountable for all aspects of the work: All authors

AUTHORS' DISCLOSURES OF POTENTIAL CONFLICTS OF INTEREST

The following represents disclosure information provided by authors of this manuscript. All relationships are considered compensated unless otherwise noted. Relationships are self-held unless noted. I = Immediate Family Member, Inst = My Institution. Relationships may not relate to the subject matter of this manuscript. For more information about ASCO's conflict of interest policy, please refer to www.asco.org/rwc or ascopubs.org/cci/author-center.
Open Payments is a public database containing information reported by companies about payments made to US-licensed physicians (Open Payments).

Aaron Li
Employment: Pfizer

Emil Lou
Stock and Other Ownership Interests: Ryght
Honoraria: Novocure, GlaxoSmithKline, Boston Scientific, Daiichi Sankyo/UCB Japan (Inst)
Consulting or Advisory Role: Novocure, Novocure, Novocure, Novocure, Boston Scientific
Research Funding: Novocure, Intima
Travel, Accommodations, Expenses: GlaxoSmithKline
Uncompensated Relationships: Minnetronix Medical, NomoCan, Caris Life Sciences

No other potential conflicts of interest were reported.

REFERENCES

1. Wang X-Y, Zhang R, Han J-H, et al: Early circulating tumor DNA dynamics predict neoadjuvant therapy response and recurrence in colorectal liver metastases: A prospective study. Ann Surg Oncol 30:5252-5263, 2023
2. Khan KH, Cunningham D, Werner B, et al: Longitudinal liquid biopsy and mathematical modeling of clonal evolution forecast time to treatment failure in the PROSPECT-C phase II colorectal cancer clinical trial. Cancer Discov 8:1270-1285, 2018
3. Tie J, Kinde I, Wang Y, et al: Circulating tumor DNA as an early marker of therapeutic response in patients with metastatic colorectal cancer. Ann Oncol 26:1715-1722, 2015
4. Garlan F, Laurent-Puig P, Sefrioui D, et al: Early evaluation of circulating tumor DNA as marker of therapeutic efficacy in metastatic colorectal cancer patients (PLACOL study). Clin Cancer Res 23:5416-5425, 2017
5. Patelli G, Mauri G, Tosi F, et al: Circulating tumor DNA to drive treatment in metastatic colorectal cancer. Clin Cancer Res:OF1-OF10, 2023
6. Abbosh C, Birkbak NJ, Wilson GA, et al: Phylogenetic ctDNA analysis depicts early-stage lung cancer evolution. Nature 545:446-451, 2017
7. Zhao X, Dai F, Mei L, et al: The potential use of dynamics changes of ctDNA and cfDNA in the perioperative period to predict the recurrence risk in early NSCLC. Front Oncol 11:671963, 2021
8. Assaf ZJF, Zou W, Fine AD, et al: A longitudinal circulating tumor DNA-based model associated with survival in metastatic non-small-cell lung cancer. Nat Med 29:859-868, 2023
9. Yang X, Zhuo M, Ye X, et al: Quantification of mutant alleles in circulating tumor DNA can predict survival in lung cancer. Oncotarget 7:20810-20824, 2016
10. Sanz-Garcia E, Zhao E, Bratman SV, et al: Monitoring and adapting cancer treatment using circulating tumor DNA kinetics: Current research, opportunities, and challenges. Sci Adv 8:eabi8618, 2022
11. Parikh AR, Mojtahed A, Schneider JL, et al: Serial ctDNA monitoring to predict response to systemic therapy in metastatic gastrointestinal cancers. Clin Cancer Res 26:1877-1885, 2020
12. Riediger AL, Dietz S, Schirmer U, et al: Mutation analysis of circulating plasma DNA to determine response to EGFR tyrosine kinase inhibitor therapy of lung adenocarcinoma patients. Sci Rep 6:1-8, 2016
13. Husain H, Melnikova VO, Kosco K, et al: Monitoring daily dynamics of early tumor response to targeted therapy by detecting circulating tumor DNA in urine. Clin Cancer Res 23:4716-4723, 2017
14. Schreuer M, Meersseman G, van Den Herrewegen S, et al: Applications for quantitative measurement of BRAF V600 mutant cell-free tumor DNA in the plasma of patients with metastatic melanoma. Melanoma Res 26:157, 2016
15. Lo YMD, Leung S-F, Chan LYS, et al: Kinetics of plasma Epstein-Barr virus DNA during radiation therapy for nasopharyngeal carcinoma. Cancer Res 60:2351-2355, 2000
16. Chen K, Zhao H, Shi Y, et al: Perioperative dynamic changes in circulating tumor DNA in patients with lung cancer (DYNAMIC). Clin Cancer Res 25:7058-7067, 2019
17. Wan JCM, Massie C, Garcia-Corbacho J, et al: Liquid biopsies come of age: Towards implementation of circulating tumour DNA. Nat Rev Cancer 17:223-238, 2017
18. Vidal J, Fernández-Rodríguez MC, Casadevall D, et al: Liquid biopsy detects early molecular response and predicts benefit to first-line chemotherapy plus cetuximab in metastatic colorectal cancer: PLATFORM-B study. Clin Cancer Res 29:379-388, 2023
19. Magbanua MJM, Brown Swigart L, Ahmed Z, et al: Clinical significance and biology of circulating tumor DNA in high-risk early-stage HER2-negative breast cancer receiving neoadjuvant chemotherapy. Cancer Cell 41:1091-1102.e4, 2023
20. Leung SF, Chan KCA, Ma BB, et al: Plasma Epstein–Barr viral DNA load at midpoint of radiotherapy course predicts outcome in advanced-stage nasopharyngeal carcinoma. Ann Oncol 25:1204-1208, 2014
21. Chera BS, Kumar S, Beaty BT, et al: Rapid clearance profile of plasma circulating tumor HPV type 16 DNA during chemoradiotherapy correlates with disease control in HPV-associated oropharyngeal cancer. Clin Cancer Res 25:4682-4690, 2019
22. Lv J, Chen Y, Zhou G, et al: Liquid biopsy tracking during sequential chemo-radiotherapy identifies distinct prognostic phenotypes in nasopharyngeal carcinoma. Nat Commun 10:3941, 2019
23. Rachman T, Bartlett D, LaFramboise W, et al: Modeling the effect of spatial structure on solid tumor evolution and circulating tumor DNA composition. Cancers 16:844, 2024
24. Fonseca NM, Maurice-Dror C, Herberts C, et al: Prediction of plasma ctDNA fraction and prognostic implications of liquid biopsy in advanced prostate cancer. Nat Commun 15:1828, 2024
25. Avanzini S, Kurtz DM, Chabon JJ, et al: A mathematical model of ctDNA shedding predicts tumor detection size. Sci Adv 6:eabc4308, 2020

26. van Leeuwen CM, Oei AL, Crezee J, et al: The alfa and beta of tumours: A review of parameters of the linear-quadratic model, derived from clinical radiotherapy studies. Radiat Oncol 13:96, 2018
27. Fowler JF: The linear-quadratic formula and progress in fractionated radiotherapy. Br J Radiol 62:679-694, 1989
28. McLaren DB, Aitman TJ: Redefining precision radiotherapy through liquid biopsy. Br J Cancer 129:900-903, 2023
29. Rostami A, Lambie M, Yu CW, et al: Senescence, necrosis, and apoptosis govern circulating cell-free DNA release kinetics. Cell Rep 31:107830, 2020
30. Muhanna N, Eu D, Chan HHL, et al: Cell-free DNA and circulating tumor cell kinetics in a pre-clinical head and neck Cancer model undergoing radiation therapy. BMC Cancer 21:1075, 2021